Bioorganic & Medicinal Chemistry Letters 27 (2017) 4471–4477

Contents lists available at ScienceDirect

Bioorganic & Medicinal Chemistry Letters

journal homepage: www.elsevier.com/locate/bmcl

1-Thiazol-2-yl-N-3-methyl-1H-pyrozole-5-carboxylic acid derivatives as antitumor agents

Alan B. Cooper [a,*], Stephane Ciblat [b], Gerald Shipps [c], Jedd Levine [a], Matthew Kostura [a], Vibha Oza [a], Lea Constantineau-Forget [b], Martin Dery [b], Chantal Grand-Maitre [b], Nicolas Bruneau-Latour [b], Edith Bellavance [b], Arshad Siddiqui [b], Michael Luther [a]

[a] Bantam Pharmaceutical, New York, NY, United States
[b] Paraza Pharma, Montreal, QC, Canada
[c] Shire PLC, Lexington, MA, United States

ARTICLE INFO

Article history:
Received 20 June 2017
Revised 31 July 2017
Accepted 2 August 2017
Available online 2 August 2017

Keywords:
Tumor cell inhibitor
Hemaopoietic cell lines
BJAB
G0/G1 cell cycle
B-cell lymphoma
SAR
1-Thiazol-2-yl-N-3-methyl-1H-pyrazole-5-carboxylic acid

ABSTRACT

A class of substituted 1-thiazol-2-yl-N-3-methyl-1H-pyrozole-5-carboxylic acid derivatives was found to have potent anti-proliferative activity against a broad range of tumor cell lines. A compound from this class (**14**) was profiled across a broad panel of hematologic and solid tumor cancer cell lines demonstrating cell cycle arrest at the G0/G1 interphase and has potent anti-proliferative activity against a distinct and select set of cancer cell types with no observed effects on normal human cells. An example is the selective inhibition of human B-cell lymphoma cell line (BJAB). Compound **14** was orally bioavailable and tolerated well in mice. Synthesis and structure activity relationships (SAR) in this series of compounds are discussed.

The pathogenesis, growth, and progression of multiple hematologic and solid tumor malignancies are characterized by aberrant regulation of cell cycle control and cellular metabolism and translation. A novel chemotype was identified while profiling modifications to an ascribed eIF4E inhibitor, 4EGI-1.[1] This chemotype shows potent anti-proliferative activity in BJAB cells, a B-cell lymphoma cell line that has been described as a diffuse large B-cell lymphoma of the germinal center B-cell (GCB) subtype from gene expression profiling studies.[2] This class of compounds also shows selective G0/G1 cell cycle arrest, induces apoptosis in BJAB cells, and modulates cancer cell metabolism characterized by decreased glutathione levels[3]-activities that have key roles in the pathogenesis of multiple hematologic malignancies and solid tumors.

Our initial approach towards the discovery of this series was founded using a structure based drug design (SBDD)[4] approach as well as a published compound and structure of 4EGI-1 (**1**) and eIF4E, respectively.[5] The chemical starting point, 4EGI-1 (**1**), is a small molecule compound that was described in the literature as an inhibitor of eIF4E, an mRNA translation initiation factor that is the rate limiting step in translation and important for regulating selective translation of key genes involved in tumorigenesis.[6,7] In our efforts to optimize and generate improved leads devoid of a hydrazine group found in 4EGI-1 (Fig. 1) and with improved physico-chemical properties, we discovered a lead series of pyrazolothiazoles **3** with improved ability to inhibit BJAB cell proliferation, but no inhibition of eIF4E.[8] The compound series had superior *in cellula* activity when compared to the parent. This led to the identity of compound **14** that was further profiled for cell inhibitory and DMPK properties.

In an effort to explore SAR and improve potency of this compound series, we profiled compounds in an antiproliferation assay using BJAB cells. The initial strategy focused on keeping the 4-(1,2-dichloro)phenyl group constant while modifying the groups attached to the 4-pyrazole ring. The methyl ester (**4**) (Fig. 2) showed minimal cell activity when profiled against the BJAB cell line. Introduction of a thioethyl & thioisopropyl group at the 5-position of the thiazole ring (**5, 6**) improved the anti-proliferation activity BJAB by approximately 3.5-fold. Removal of the ester group to give (**7, 8**) showed a further 2 and 5-fold improvement demonstrating the importance of a carboxyl group at the 5-pyrazole position. Removal of the benzyl-CH_2 to give (**9**) showed

* Corresponding author.
E-mail address: acooper@bantampharma.com (A.B. Cooper).

http://dx.doi.org/10.1016/j.bmcl.2017.08.003
0960-894X/

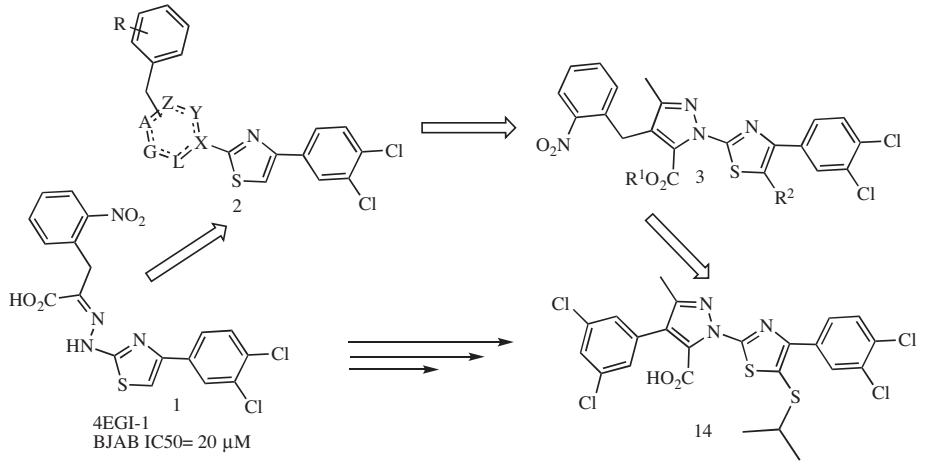

Fig. 1. Design of pyrazolo-thiazole core based on 4EGI-1.

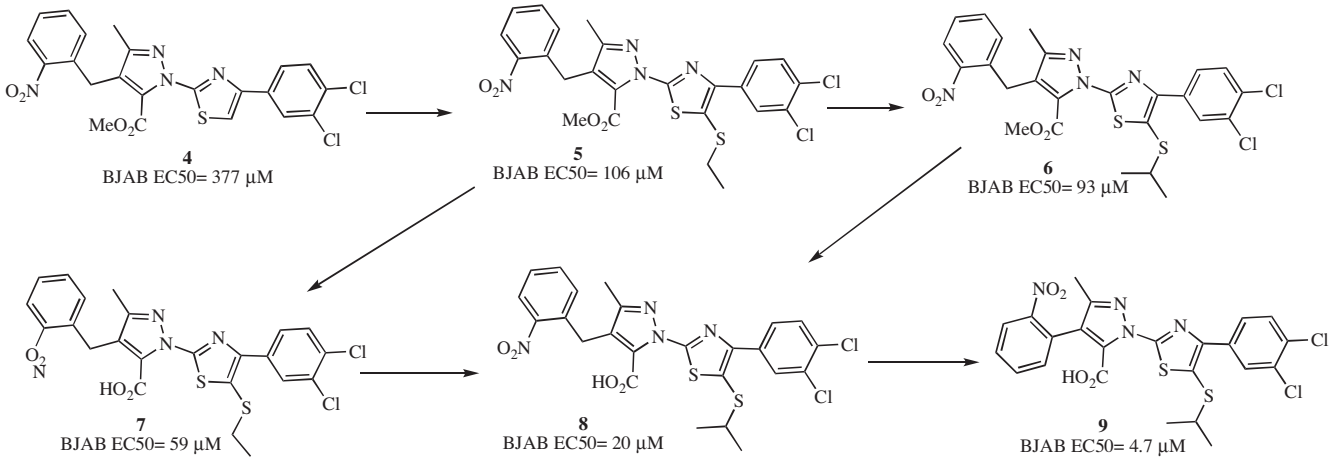

Fig. 2. Initial modifications.

another 4-fold improvement resulting in a compound with single digit μM inhibition. The 4-1,2-dichlorophenyl group that was originally part of the 4EGI-1 molecule, was therefore kept constant while modifying the aryl groups attached to the 4-pyrazole ring. It is worth noting that changing the position of thiazole attachment to the 2-N-pyrazole ring position resulted in a 3-fold loss in activity (not shown) and therefore this point of attachment was abandoned.

Based on these results, we concentrated our SAR development on modifications of the aryl groups attached to the 4-position of the pyrazole ring. A general synthetic scheme is shown in Fig. 3. Starting material **A** was treated with *n*-butyl lithium followed by dithioisopropyl ether to obtain the thioisopropyl compound **B.** Treatment with hydrazine hydrochloride and base gave the hydrazine **C**. Formation of the pyrazole ring **D** was accomplished by the addition of methyl (*Z*)-2-(methoxyimino)-4-oxopentanoate to the hydrazine **C**. This was followed by bromination to obtain the main intermediate, di-bromo compound **E**. The di-bromo intermediate **E** was then selectively arylated under Suzuki cross-coupling[9] conditions at the 4-position of the thiazole ring to yield the arylated

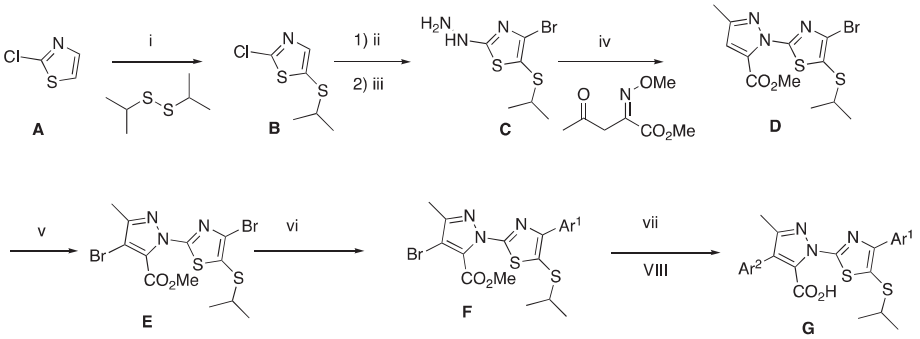

Fig. 3. Reagents: i. *n*-BuLi, THF −78 °C, 29%; ii. Br_2, DCM, 77%; iii. $NH_2NH_2{\cdot}HCl$, DIPEA, NMP, 88%; iv. HCl, MeOH, reflux, 39%; v. Br_2, DCM, 61%; vi. Ar^1-$B(OH)_2$, Pd (dtbdf)Cl_2, K_2CO_3, THF, 90 °C; vii. Ar^2-$B(OH)_2$, $Pd(PPh_3)_4$, Na_2CO_3, 1,4-dioxane, H_2O followed by hydrolysis; viii. KOH, 80% MeOH/H_2O.

Table 1
Modification of the aryl group on the pyrazole ring.

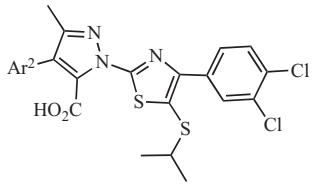

Compound #	Ar^2	BJAB EC_{50} (μM)
9	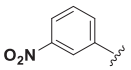	4.7
10		3.4
11	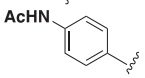	139
12	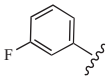	0.9
13	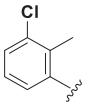	5.1
14	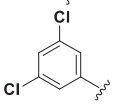	0.554
15	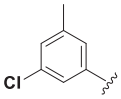	0.663
16	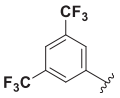	1.8
17	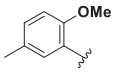	9.5
18	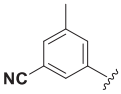	4.8
19	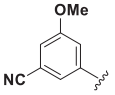	5.2
20	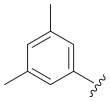	2.7
21	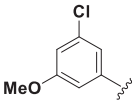	0.76
22	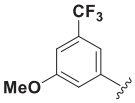	1.38
23	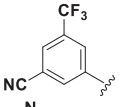	3.6
24		22.0
25		14.0

Table 1 (*continued*)

Compound #	Ar^2	BJAB EC_{50} (μM)
26		12.0
27		5.9
28	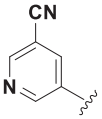	20.0
29	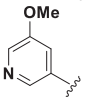	21.0
30	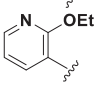	11.0
31	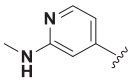	18.0
32	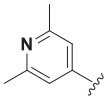	0.580
33	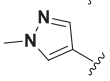	6.8

compound **F**. This was followed by another Suzuki reaction at the 4 position of the pyrazole ring to give **G**. In this way, we were able to selectively introduce various aryl and heteroaryl rings at the desired positions of the molecule.

With a general synthesis in hand, we modified the aryl (Ar^2) group at the 4 position of the pyrazole ring as shown in Table 1. We retained the ability to inhibit cell proliferation when the nitro group on the aryl ring (**10**) was removed. Introduction of a *m*-fluoro substitution on the phenyl ring resulted in the first sub micromolar compound (**12**). However, introduction of a para acetamido group (**11**) resulted in ~35-fold reduction in activity. We then looked at further di-substitution of the phenyl ring since the unsubstituted phenyl compound **10** and *m*-fluoro substitution **12** were found to be the most active. The *o*-methyl-*m*-chloro substitution (**13**) was 14-fold less active than (**15**) bearing the corresponding di-meta substitution. This constituted the first example of a sub μM di-substituted compound with an EC_{50} = 0.663 μM providing the rationale for continued di-meta substitution. The most potent di-meta substituted phenyl compound was **14** with an EC_{50} = 0.554 μM.

The phenyl ring could also be substituted for a 4-pyridine ring (**27**) with retained cell activity. Moving the nitrogen on the pyridine ring to the 3-position (**26**) resulted in approximately a 4-fold loss in activity. Introduction of another nitrogen in the ring to give a pyrimidine (**24**) and pyrazine (**25**) ring also resulted in loss of activity. We therefore looked at various pyridine substitutions. Mono 2 and 3 substitution on the pyridine ring gave only double digit μM inhibitory cell activity. However, the 3,3-di-methyl substituted compound **32** gave an EC_{50} = 0.58 μM that carries along with the observation that di-meta substitution with the correct substituents on the aryl or heteroaryl ring gave the most potent compounds. We also explored several 5 membered heteroaromatic rings. The most potent 5-membered heteroaryl ring compound was the *N*-methylpyrazole ring, **33** at EC50 = 6 μM. This compound was significantly less active than the most active 6 membered ring systems with no other 5-membered ring system tested showing improved cell activity (not shown).

Several modifications to the S-isopropyl group were explored (not shown). Oxidation to a sulfone and removal of the S-isopropyl group were not tolerated. Removal of the sulfur to give an isobutyl group was tolerated.

Since the phenyl ring substitutions were the most active and tolerated substitution, we next looked at ortho, meta and para substitutions around the phenyl ring. As can be seen in Table 2 both ortho and meta substitution with methyl and trifluoro methyl groups gave equipotent compounds. Para substitution resulted in a 3–4-fold loss in activity. Both OMe and Cl substitution were favored at the meta position.

As compound **14** was one of the most potent compounds, we looked at several modifications to the aryl (Ar^1) group at the 4 position of the thiazole ring while keeping the *m*-dichlorophenyl group on the pyrazole ring constant as shown in Table 3. As observed, changing the di-chloro substitution from *meta-para* to di-*meta* (**47**) reduced the cell potency by 4-fold. Further modification to give *o*-fluoro-*m*-chloro (**48**) gave a further 9-fold reduction in potency. Introduction of heteroaryl groups resulted in substantial reduction in cell potency. Further modifications at this site were not tolerated.

Based on the BJAB cell proliferation EC_{50} data, compound **14** was selected for additional profiling. To better understand if the inhibition of cell proliferation was a general chemtoxic or chemostatic effect, or a specific pathway or target(s) we profiled the compound across a panel of 99 different hematologic and solid tumor cancer cell lines. The results demonstrated that compound **14** has a potent anti-proliferative activity against a select, but distinct subset of these cancer cells while not having any observed effects on normal human cells. A representation of a subset of compound **14** effects on various cell line growth inhibitory activity are denoted in Table 4 and Fig. 4. As can be seen in Fig. 4, compound **14** had major inhibitory activity on hemaopoietic cell lines.

In our effort to understand the mechanism of action behind the distinct and select set of antiproliferative activity observed for our lead compound **14**, we used high content imaging to examine various cellular activities involved in cell transformation. In order to do these studies, we selected a solid tumor cell line (HCT-116) from Table 4. This cell line was ideal for high content cell imaging studies as it undergoes quiescence upon treatment with compound **14** in contrast to hematopoietic cell lines, such as BJAB, that undergo rapid apoptosis (data not shown). The ability to understand in depth different cell biology features is difficult in apoptotic cells. Thus, we chose the HCT-116 cell line to profile compounds versus the various hallmarks of cancer cell biology including, but not limited to, cell cycle effects, DNA damage,

Table 3
4-Aryl substitution on the thiazole ring.

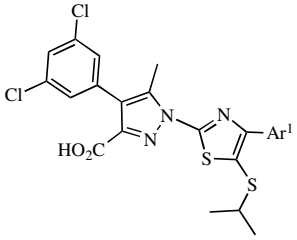

Compound #	Ar^1	BJAB EC_{50} (μM)
14	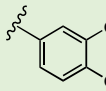	0.554
47	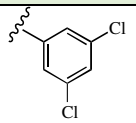	2.0
48	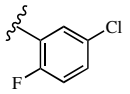	4.8
39		No inh
50		No inh
51		>44
52	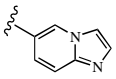	No inh
53	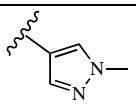	No inh

The shades in green were meant to highlight the most active in the series.

Table 2
ortho, *meta* and *para* phenyl substitution.

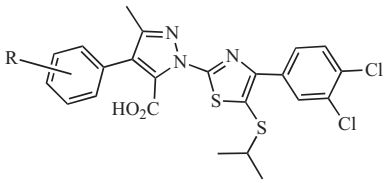

R	BJAB EC_{50} (μM)		
	ortho para		*meta*
H	3		
Me	5.5	3.8	17.0
CF_3	5.2	3.5	22.0
OMe	14.7	2.1	14.0
Cl	13.1	2.5	13.6

Table 4
Sample cell line inhibition data.

Cell Line	Tumor Type	IC50 (μM)
SU-DHL-10	Diffuse Large B-cell Lymphoma	0.43
Jurkat	T cell leukemia	0.5
Daudi	Burkitt's lymphoma	0.38
TC-71	Ewing's Sarcoma	0.29
HCT-116	Colorectal	0.6
A2780	Ovarian	0.29
NCI-H460	Lung (large cell)	0.33
MDA-MB-469	Breast	1.57
MIA PaCa-2	Pancreatic	0.32
MCF-7	Breast	0.26
MCF10A	Non-malignant Human Mammary Epithelial	35.0
Primary B Cells		>40

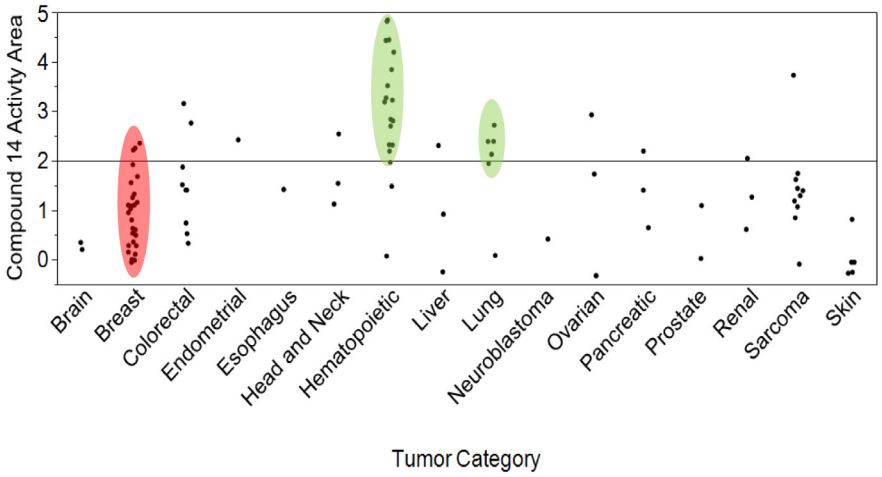

Fig. 4. Cell line evaluation: Compound 14 was tested against a panel of 99 hematopoietic and solid tumor lines. Compounds were tested at eight dilutions (n = 3) and IC_{50} and activity area value calculated for each cell line. The data represent the outcome of tests using compound 14. The reference line indicates the mean activity area line above which was considered a positive outcome.

oxidative phosphorylation, mitophagy, autophagy and cellular metabolism as well as other cancer associated cell activities. In this ongoing exploration, for the purposes of this manuscript, we share here our learning in the areas of cell cycle. Other findings and results will be published in due course (data not shown).

Treatment of HCT-116 cells with cell active compounds **25** and **14** that had anti-proliferative activity resulted in a specific cell-cycle arrest (Fig. 5). Cells were identified as being arrested largely at the B0/G1 interphase with a concomitant reduction in S-G2 and M phase cells. The effect is both dose and time dependent with greater reduction in S-phase cells occurring at 24 h, consistent with the doubling time of HCT-116 cells (18 h; data not shown). The same effect was not seen with the inactive analog compound **11**. The effect on G1 progression suggests that the compounds affect cell cycle progression during a critical part of the cell cycle where growth factor and nutrient control play a key role in

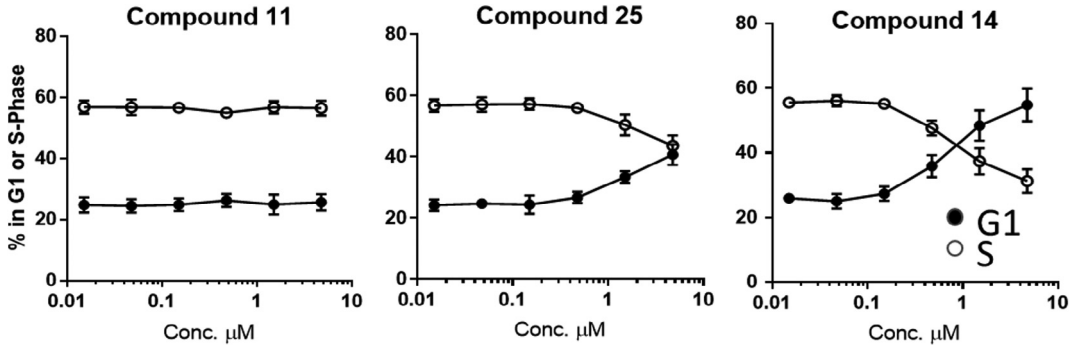

Fig. 5. Cell cycle analysis of Compound **11**, **14,** and **25**. HCT 116 cells were treated for 24 h with compound and measured for DNA content, DNA synthesis and levels of phosphorylated histone H3. Briefly, HCT-116 cells were plated into black-walled poly-L-lysine coated microclear tissue culture plates and incubated overnight. Cells were treated with compound dissolved in DMSO and diluted into McCoys modified media with 10% fetal bovine serum. The cells were incubated with compound for 24 h after which they were treated with EdU to label newly synthesized DNA and allow for positive identification of S-phase cells[10] then fixed with 4% formaldehyde. Following fixation, EdU incorporation was detected according to the manufacturer's instructions (Thermo Fisher). The labeled and stained cells were imaged using an ArrayScan XTi High Content Imager with a 20×/0.4NA Plan-Neofluar objective using three fluorescent channels. Image analysis was performed using Cellomics HCS Studio software. Cell cycle classification and statistical analysis was performed using Knime. The output of the image analysis is: total number of cells per well, total DNA content, specific identification of cells in S-Phase (EdU staining). All datapoints shown are means of three biological replicates. Error bars represent the standard error of the mean of the three biological replicates.

Table 5
In vitro and *in vivo* DMPK data.

In vitro DMPK Data		*In vivo* Mouse PK			
Kinetic solubility[11]	40.2 μM	Oral		IV	
Human hepatocyte Cl	12.4 mL/min/kg	C_{max}	1321.4	C_0	3185.5 ng/mL
Human/mouse protein binding	97.3%/99.2%	t_{max}	5 h	$T_{1/2}$	8 h
Caco-2 A > B/B > A	7.6/2.8	$AUC_{0\text{-inf}}$	25801.6 ng/mL*h	$AUC_{0\text{-inf}}$	10661.4 ng/mL*h
		%F	48.4%	CL	0.8 mL/min/kg
				V_{ss}	444.4 mL·kg

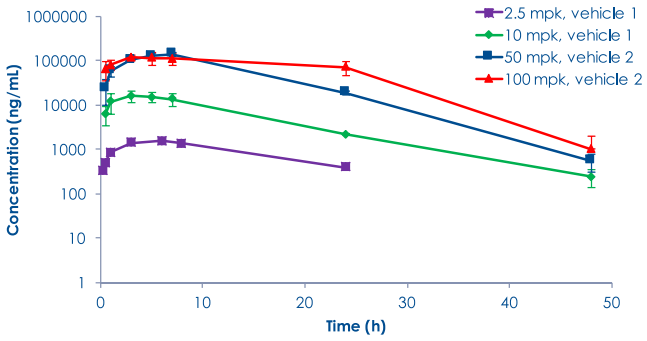

Fig. 6. Single rising dose mouse PK.

determining whether cells divide. This restriction point is well defined and regulate cell cycle entrance into S-phase in the absence of necessary nutrients and growth factors. The specific mechanism by which compound **14** inhibits G1 progression is currently being explored (data not shown).

Given the distinct pattern of anti-tumor activity and this potent effect on cell cycle arrest, we moved to better assess a subset of these compounds *in vivo*. As a first step, we profiled a subset of compounds for *in vitro* pharmacokinetic (PK) assessment which resulted in the prioritization of compound **14** for additional *in vivo* assessment. Shown in Table 5, compound **14** showed 40 μM kinetic solubility at pH 7.4, in phosphate buffer that was improved to >200 μM upon addition of 10% FBS, suggesting that this compound was potentially highly protein bound. Indeed, human protein binding was 97.3% while mouse protein binding was 99.2%. Caco-2 data suggested the possibility of good *in vivo* oral absorption. Human hepatocyte clearance was low at 12.4 mL/min/kg. Based on the *in vitro* assessment, we moved forward with compound **14** to asses further the pharmacokinetics *in vivo* in mouse. The PK data, summarized in Table 5, show that compound **14** gave an acceptable PK profile with 48.4% bioavailability and a $T_{1/2}$ of 8 h. Clearance was low at 0.8 mL/min/kg, with an acceptable volume of distribution.

A single rising dose PK experiment, summarized in Fig. 6 and Table 6, show a supra-proportional increase in Cmax and AUC between 2.5, 10 and 50 mg/kg doses. At 100 mg/kg the plasma levels plateaued until 24 h.

Maximum tolerated dose (MTD) studies with compound **14** were undertaken in preparation for further profiling in tumor xenograft mouse models.[12] Compound **14** was administered daily orally at 10, 30 and 60 mg/kg. After 7 consecutive days of treatment, no adverse effects attributable to the drug itself were recorded. In a final attempt to trigger toxic effects, higher doses of **14** were administered to the mid and high-dose groups (90 mg/kg and 120 mg/kg, respectively) for 5 additional days. Despite this MTD protocol modification, no critical clinical observations were recorded over the entire study duration. Gross pathology on animals performed 48 h after the last administered dose did not reveal any changes in organ weights or organ damages. As stated, BTM-1516 did not induce toxicity at doses up to 120 mg/kg orally daily. Notably, there were no significant differences in drug exposure and Cmax 90 vs. 129 mg/kg. Induction of clearance was observed at all tested drug concentrations. Hepatocellular hyperplasia was only found statistically significant in the highest dose group (120 mg/kg). Taken together, these results suggest that the maximum tolerated BTM-1516 dose in mice, when given orally daily, is approximately 90 mg/kg.[13] The mean plasma concentration levels are summarized in Table 7.[14]

In conclusion we accomplished a >650 fold improvement in BJAB cell inhibition by modifying the aryl groups at the 4-positions of both rings on the 2-(1H-pyrazol-1-yl)thiazole bis-aryl ring system. Introduction of an S-isopropyl group at the 5-position of the thiazole ring with concomitant generation of a carboxyl group at the 5-position of the pyrazole ring to generated compound **14**. Compound **14** thus shows good potency in our primary cellular assay, acceptable *in vitro* and *in vivo* PK and offers an initial understanding of its mechanism of action which is being further elucidated in our labs. Currently efforts are underway to assess this a compound in the BJAB cell line model of lymphoma as well as to understand its mechanism of action. To that end, we are assessing it for its effect on cellular metabolism as well as autophagy. Our current efforts are focused on profiling compound **14** and additional compounds in this series to better understand both the mechanism of action as well as the putative target via which it lends its biological anti-tumor effect that will be published in due course.

Table 6
Single rising dose mouse PK.

Dose (mg/mL)	Fold Increase	C_{max} (ng/mL)	Observed fold-increase C_{max}	$AUC_{0\text{-}inf}$ (ng/ml*h)	Observed Fold-Increase AUC_{inf}	MRT Oral (h)
2.5	–	1321	–	25802	–	15.1
10	4	15,744	11.9	257,275	10	10.1
50	5	137,813	8.8	2,247,240	8.7	9.3
100	2	130,551	0.9	2,122,592	1.4	14.3

Table 7
Mean plasma concentration (ng/mL).

Group	C_{7h}-Day 1	C_{min}-Day 3	C_{7h}-Day 5	C_{min}-Day 7
B-10 mpk	19706 ± 4670	3029 ± 1396	18164 ± 2505	1347 ± 352
C-30 mpk	63616 ± 23873	3499 ± 552	57291 ± 23897	1710 ± 1148
D-60 mpk	88839 ± 11445	9012 ± 1015	79821 ± 13041	1177 ± 111
Dose	C_{max}	C_{max}–D	$AUC_{0\text{-}inf}$ (ng/mL*h)	$AUC_{0\text{-}inf}$+D
10 mpk	28,978.9	2,897.9	330,000.0	33,000.0
90 mpk	134,485.3	1,494.3	1,485,193.5	16,502.2
120 mpk	127,982.8	1,066.5	1,537,624.9	12,813.6

Acknowledgements

We thank the Bantam Pharmaceutical Board Members Victor F. Keen, Lionel Goldfrank III, and W. James Tozer, Jr. for their support and encouragement. We would also like to thank the employees of Paraza Pharma, Inc. and Scitovation for their support and work on this project.

References

1. Sekiyama N, Arthanari H, Papadopoulos E, Rodriguez-Mias RA, Wagner G, Léger-Abraham M. Molecular mechanism of the dual activity of 4EGI-1: dissociating eIF4G from eIF4E but stabilizing the binding of unphosphorylated 4E-BP1. *Proc Natl Acad Sci U S A*. 2015;112:E4036–4045.
2. Pfeifer M, Grau M, Lenze D, et al. PTEN loss defines a PI3K/AKT pathway-dependent center subtype of diffuse large B-cell lymphoma. *PNAS*. 2013;110:12420–12425;
Wilson WH, Young RM, Schmitz R, et al. Targeting Bcell receptor signaling with ibrutinib in diffuse large B cell lumphoma. *Nature*. 2015;21:922–927.
3. Kostura M, Levine J, Oza V, et al. BTM-3528 potently induces G1/G0 cell cycle arrest and is efficacious in pre-clinical models of diffuse large B-cell lymphoma. Proceedings of 2nd AACR Conference on Hematologic Malignancies: Translating Discoveries to Novel Therapies. 2017, Abstract 45, 63.
4. Lounnas V, Ritschel T, Kelder J, McGuire R, Bywater RP, Foloppe N. Current progress in structure-based rational drug design marks a new mindset in drug discovery. *Comput Struct Biotechnol J*. 2013;5. Article e201302011.
5. Papadopoulos E, Jenni S, et al. Structure of the eukaryotic translation initiation factoreIF4E in complex with 4EGI-1 reveals an allosteric mechanism for dissociating eIF4G. *PNAS*. 2014;111:E3187–E3195.
6. Moerke NJ, Aktas H, Chen H, et al. Small-molecule inhibition of the interaction between the translation initiation factors eIF4E and eIF4G. *Cell*. 2007;128:257–267.
7. Yefidoff-Freedman R, Chen T, Sahoo R, et al. 3-substituted indazoles as configurationally locked 4EGI-1 mimetics and inhibitors of the eIF4E/eIF4G interaction. *Chembiochem Eur J Chem Biol*. 2014;15:595–611.
8. Supporting data will be reported in subsequent publications.
9. Gujral SS, Khatri S, Riyal P. Suzuki cross coupling reaction-a review. *Indo Global J Pharma Sci*. 2012;2:351–367.
10. Salic A, Mitchison TJ. A chemical method for fast and sensitive detection of DNA synthesis in vivo. *Proc Natl Acad Sci*. 2008;105:2415–2420.
11. Kinetic solubility was carried out in PBS buffer at pH = 7.4.
12. Mouse xenograft tumor model studies to be reported in future communications.
13. MTD experimental design: J:Nu mice were dosed at 10, 30 and 60 mpk PO QD. Group C increased to 90 mpk from day 8 to 13 and group D increased to 120 mpk from day 8 to 13.N = 4 in each dosing group. Clinical signs and body weights recorded every day, blood samples taken every other day (Cmax and predose alternation) followed by a 48 h sampling schedule after the last dose on day 7. Necropsy on day 9 and spleen and liver weights recorded.
14. MTD experimental design: J:Nu female mice were dosed at 10, 30 and 60 mpk PO QD in a formulation consisting of 5% NMP, 10% PEG-400, 15% Solutol and 70% D5W. The 30 mg/kg dose increased to 90 mpk from day 8 to 13 and the 60 mg/kg dose increased to 120 mpk from day 8 to 13-N = 4 in each dosing group. Clinical signs and body weights recorded every day, blood samples taken every other day (Cmax and predose alternation) followed by a 48 h sampling schedule after the last dose on day 7. Necropsy on day 9 and spleen and liver weights recorded.